

# Holographic Plasma Lenses

M. R. Edwards,<sup>1,\*</sup> V. R. Munirov,<sup>2</sup> A. Singh,<sup>2</sup> N. M. Fasano,<sup>3</sup> E. Kur,<sup>1</sup> N. Lemos,<sup>1</sup> J. M. Mikhailova,<sup>3</sup> J. S. Wurtele,<sup>2</sup> and P. Michel<sup>1</sup>

<sup>1</sup>*Lawrence Livermore National Laboratory, Livermore, California 94550*

<sup>2</sup>*University of California at Berkeley, Berkeley, California 94720*

<sup>3</sup>*Princeton University, Princeton, New Jersey 08544*

(Dated: June 1, 2021)

A hologram fully encodes a three-dimensional light field by imprinting the interference between the field and a reference beam in a recording medium. Here we show that gas-density plasma supports transmission holograms and that two collinear pump lasers with different foci overlapped in a gas jet produce a plasma zone plate, a holographic lens capable of focusing or collimating a probe laser at intensities several orders-of-magnitude higher than the limits of a non-ionized optic. We outline the theory of these diffractive plasma lenses and present simulations for two plasma mechanisms that allow their construction: spatially varying ionization and ponderomotively driven ion-density fluctuations. Damage-resistant plasma optics are necessary for manipulating high-intensity light, and divergence control of high-intensity pulses — provided by holographic plasma lenses — will be a critical component of high-power plasma-based lasers.

Holograms record both the phase and the amplitude of light, allowing the complete reconstruction of a light field at a later time [1]. A hologram is created by capturing the interference between a signal beam and a reference beam in a light-sensitive medium, e.g. a photographic plate; a delayed second reference beam diffracts to reproduce the signal beam. The interference is commonly mapped to attenuation, but the pattern may also be embedded as a phase shift [2]: a variation of the refractive index's real component. In principle, any medium where the index of refraction is modified by the intensity of light can store a hologram, but current optics rely on a limited collection of solid-state materials. The index of refraction ( $n$ ) of a plasma ( $n < 1$ ) differs from that of both vacuum ( $n = 1$ ) and neutral gas at similar density ( $n > 1$ ), and the formation and density evolution of plasma may be driven by light, suggesting that we can create a hologram by modulating plasma density with lasers.

The damage threshold of a plasma is orders-of-magnitude higher than that of a solid-state optic; plasma optics use this to manipulate light at extreme intensities [3]. Possible plasma devices include amplifiers to increase power [4–7], gratings [8–11] and mirrors [12, 13] to redirect beams, and waveplates [14–16] and Pockels cells [17] to manipulate polarization. However, the only demonstrated solutions for focusing light above  $10^{12} \text{ W/cm}^2$  are the concave plasma mirror [18] and compound parabolic concentrator [19], neither of which is well-suited to high-repetition-rate experiments. A viable plasma hologram offers an exciting alternative. The hologram of a point source is a sinusoidal zone plate — a type of diffractive lens invaluable for focusing x rays [20] — so two pump lasers configured to provide a plane wave and a spherical wave, or two spherical waves with different radii, can drive an index modulation that will focus a subsequent probe. Although holograms can apply many different spatial operations, focusing and collimating are partic-

ularly useful. An efficient plasma zone plate would allow collimation of high-intensity light for high-order harmonic generation [21] and filamentation [22] experiments or improve the focusing of high-energy laser facilities (e.g. the Advanced Radiographic Capability (ARC) laser [23]). Previous efforts to design plasma holograms have used reflective surface [24] and reflective volume [25] approaches, which require high-quality surfaces and high (near-solid) plasma density, restricting viability for high-repetition-rate systems, or electron plasma waves [26], which are both short-lived and unable to withstand probe intensities higher than the driving pump.

In this letter, we propose a new plasma lens concept based on transmission volume holograms constructed either via spatially varying ionization (SVI) or by ponderomotively driven ion waves. Both SVI, where only regions of constructive interference between two pump lasers are ionized and ion gratings, driven in a fully-ionized plasma by the ponderomotive force of a modulated pump intensity profile, have been used to generate high-flux volume gratings [8, 10, 27–30]. The performance and potential applications of volumetric diffraction-based optics are governed by the achievable magnitude of refractive index modulation ( $\Delta n$ ); here  $\Delta n$  represents the peak-to-peak amplitude of a spatially-varying refractive index:  $n(\mathbf{x}) = n_0 + \delta n(\mathbf{x})$ . Ponderomotive ion gratings with  $\Delta n \approx 10^{-4}$  are experimentally routine [9], and simulations readily predict conditions for which  $\Delta n > 10^{-2}$  [10, 32, 33]. For SVI,  $\Delta n \approx 10^{-2}$  arises from the difference in refractive index between plasma (ionized regions) and non-ionized gas, and although induced by femtosecond pulses, the structure may persist for tens to hundreds of picoseconds [30]. Both mechanisms produce plasma structures that are sufficiently persistent to control a probe with much longer duration than or at a substantial delay from the pump lasers, and, as we show here, need only relatively small volumes of gas-density

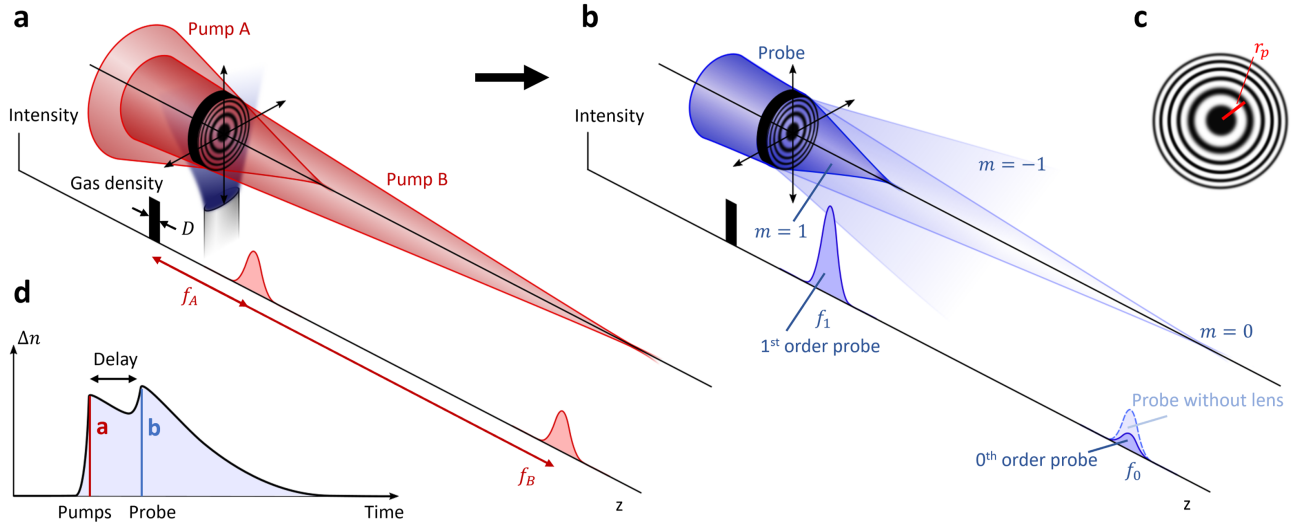


FIG. 1. Schematic of a holographic plasma lens. (a) Two pump lasers overlap in a gas (extent along  $z$  is  $D$ ), arranged so that their interference pattern is a sinusoidal zone plate. (b) At a delayed time, a probe laser passes through the resulting structure and is diffracted into one or more orders of the zone plate. (c) The intensity profile of the overlapped pumps and the resultant index modulation. (d) The peak index of refraction modulation as a function of time, showing the formation of the structure with the arrival of the pumps, followed by a decay and possible modification by the probe. The amplitude and timescale both depend on the chosen nonlinear mechanism.

plasma to create efficient transmission holograms and diffractive plasma lenses that tolerate intensities of  $10^{14}$  to  $10^{17}$  W/cm<sup>2</sup>.

Consider two collinear equal-power pump lasers ( $\alpha = A, B$ ) focused at distinct points  $f_\alpha$  along  $z$  with the f-number of each beam ( $F_\alpha$ ) chosen such that they have the same beam diameter at  $z = 0$  ( $|f_A/F_A| = |f_B/F_B|$ ), as shown in Fig. 1a. The beams propagate in vacuum aside from a region with extent  $D$  centered at  $z = 0$  where the index of refraction is intensity-dependent, a configuration that can, for example, be realized with a gas jet. For ease of analysis, we will restrict  $f_\alpha$  to be larger than the Rayleigh range so that the beams cross the gas in their near field. The two pumps interfere everywhere they overlap, but inside the gas that interference is encoded as variation of the refractive index by the dependence of  $n$  on intensity ( $I$ ), creating the index modulation of a zone plate (Fig. 1c). At a delayed time (Fig. 1d), a probe crossing the index modulation can be focused (Fig. 1b), with the plasma density potentially evolving due to both the pumps and the probe.

A zone plate consists of concentric alternating regions of opaque or phase shifting material, spaced so that transmitted light interferes constructively at the desired focal point [2, 34, 35]. The radii of boundaries between zones ( $r_p$ ) are associated with  $\lambda/2$  phase shifts of light, from which follows  $r_p^2 = p\lambda(f + p\lambda/4)$ , where  $p$  is the number of the transition,  $\lambda$  is the wavelength of the light of interest, and  $f$  is the focal length. For  $p\lambda \ll f$ ,  $r_p^2 \approx p\lambda f$ . If the pump and probe have different wavelengths ( $\lambda_p$  and  $\lambda_0$ , respectively), both must satisfy  $p\lambda \ll f$  for ef-

ficient diffraction. The size of the focal spot is governed by the number of zones ( $P$ ) as  $w_0 = \sqrt{\lambda f/4P}$ , which follows from the dependence of spot size on numerical aperture. Zone plates are highly chromatic, restricting the focusable bandwidth ( $\Delta\lambda$ ); the probe must satisfy  $\Delta\lambda/\lambda_0 \leq 1/P$  for the focal position to not shift by more than a Rayleigh range with  $\lambda$ .

For a thin lens, the thickness of the optic is set by the condition that an efficient phase-shifting zone plate has a change of refractive index between zones that creates a phase shift of order  $\pi$ :  $\Delta\phi \approx \pi = 2\pi(D/\lambda_0)\Delta n$ . For a volumetric plasma lens, the required thickness is closer to that of a Bragg grating,  $D/\lambda_0 = 1/\Delta n$ , i.e. differing by a factor of two [36]. Across all values of plate thickness, dropping leading coefficients of order 1,  $D$  is given by:

$$\frac{D}{\lambda_0} \approx \frac{1}{\Delta n}. \quad (1)$$

Taking SVI as a representative example, we will neglect absorption and note that the real part of the refractive index varies between that for plasma ( $n = \sqrt{1 - N}$  where  $N = n_e/n_c$  for plasma critical density  $n_c = \epsilon_0 m_e \omega^2 / e^2$ ) and that for the non-ionized gas, where ordinarily  $|1 - n_{\text{plasma}}| \gg |1 - n_{\text{gas}}|$ . A reasonable approximation is then  $\Delta n \approx 1 - n_{\text{plasma}} = 1 - \sqrt{1 - N} \approx N/2$  for small  $N$ . From this and the above condition on  $\Delta\phi$ , the plasma density and thickness should satisfy:  $ND \approx \lambda_0$ .

If the two pumps have intensity at  $z = 0$  such that the gas is ionized in their regions of maximum constructive interference and Eq. 1 is satisfied, a zone plate is created

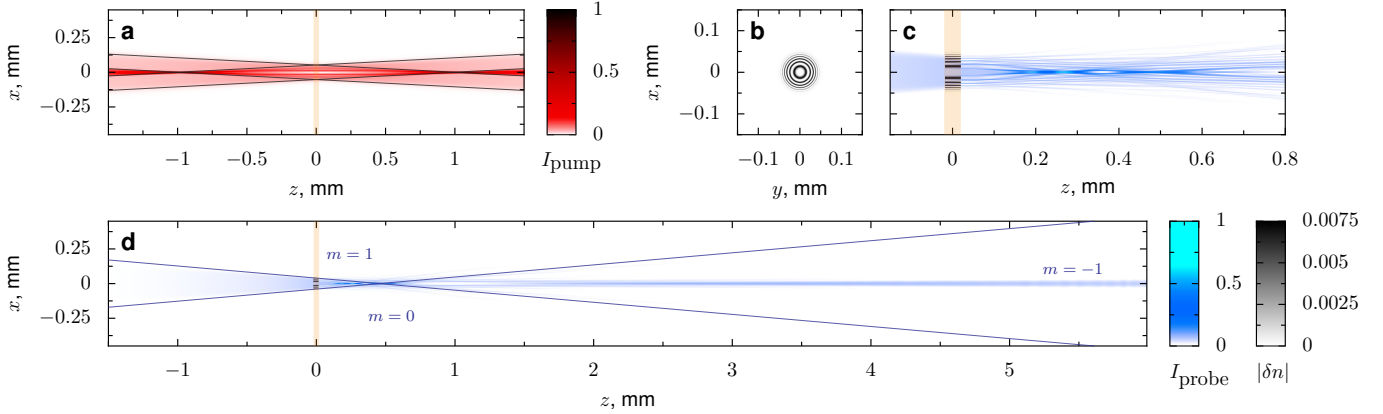


FIG. 2. Three-dimensional calculation (PPS [37]) for a thin plasma lens formed by pump lasers ( $f_A = -1$  mm,  $f_B = 1$  mm) in a 40 μm medium where  $\Delta n = 0.0075$ . The pump ( $\lambda_p = 400$  nm,  $\theta_{A,B} = 3^\circ$ ) and probe ( $\lambda_0 = 400$  nm,  $\theta = 5^\circ$ ,  $f_0 = 0.455$  mm) are arranged so that the  $m = -1$  probe order is near-collimated. (a) The pump intensity, showing the zone-plate-like interference pattern formed when the two beams are equally out of focus ( $z = 0$ ). (b) The index modulation associated with the plasma. (c) The intensity of the probe, showing the  $m = 0, 1, 2$  foci. (d) The full propagation of the probe, showing the  $m = -1$  component.

with focal length:

$$f = \frac{f_A f_B}{f_A - f_B} \cdot \frac{\lambda_p}{\lambda_0}. \quad (2)$$

A probe focused at the point  $f_0$  along the  $z$  axis, will, after passing through the plasma zone plate, have new  $m$ -order focal spots at:

$$f_m = \frac{f f_0}{f + m f_0}, \quad (3)$$

where  $f$  is given by Eq. 2 and the energy in each order is determined by the detailed spatial variation of the refractive index [37].

The importance of diffraction into higher-order focal spots varies with the thickness of the zone plate. Thin diffractive lenses ( $D\lambda_0/\delta^2 \ll 1$ , where  $\delta$  is the width of the outer-most zone) support multiple orders, whereas thick lens can produce a single well-defined spot [38]. This is analogous to the Raman-Nath and Bragg regimes for gratings (defined by  $Q = 2\pi\lambda D/(n_0\Lambda^2)$ ,  $\Lambda$  is the grating wavelength), where there are multiple diffraction orders or a single diffracted beam, respectively. For a thin zone plate where  $\delta n(I)$  is monotonic, equal energy is diffracted into positive and negative focal orders (e.g.  $m = 1$  and  $m = -1$ ), limiting total efficiency. Although for a plasma zone plate  $\delta n$  is generally a nonlinear function of  $I$  — ionization fraction is a strongly nonlinear function of intensity [39] — and the phase shift is non-sinusoidal, the first-order diffraction efficiency ( $\eta_1$ ) should fall between those of the Gabor plate ( $\delta n$  linear with intensity) and the Rayleigh-Wood phase plate (infinite nonlinearity), which are similar at  $\eta_1 = 0.34$  and  $\eta_1 = 0.41$ , respectively [2], so the exact functional form of the nonlinearity does not strongly impact the performance of a thin holographic optic.

We use a three-dimensional (3D) paraxial propagation solver (PPS) to numerically evaluate the formation and performance of a diffractive plasma lens. The solver neglects the time dynamics of the pumps and probe and considers the interaction as three separate steps: (1) linear propagation of the pumps through a uniform medium, (2) change of the refractive index as a function of pump intensity, and (3) linear propagation of the probe through the new distribution of refractive index [37]. Figure 2 shows a calculation for a probe propagating through a 40-μm thick plasma zone plate formed ( $\delta n \propto I$ , with  $\Delta n = 0.0075$ ) by two pumps with  $f_A = -1$  mm and  $f_B = 1$  mm. The zone plate has a focal length  $f = 0.5$  mm (Fig. 2b) and substantially modifies the probe focus (Fig. 2cd). The zeroth-order probe focus ( $f_0 = 0.455$  mm) is chosen so that the  $m = -1$  order is near-collimated. Figure 2c shows the residual  $m = 0$  focus of the probe, as well as the new  $m = 1$  and  $m = 2$  focal spots near  $f_1 = 0.24$  mm and  $f_2 = 0.16$  mm. The larger scale of Fig. 2d shows that significant energy is transferred to the  $m = -1$  near-collimated beam ( $f_{-1} = 5$  mm).

Although thin zone plates are analytically simpler and more common for x-ray focusing, there are clear limits on efficiency under the restriction that the phase shift is a monotonic function of intensity, which makes the creation of a true Fresnel lens difficult. In contrast, the thick zone plate regime ( $D\lambda \gg \delta^2$ ), which can be described by coupled mode theory [38], allows the redirection of most incident energy to the desired order. A thick plate can be thought of as an assembly of local gratings with varied spacing and orientation; efficiency is highest when the probe satisfies the Bragg condition for each local grating. In the PPS calculation shown in Fig. 3a, around 80% of the probe energy is within the  $m = -1$  focus;

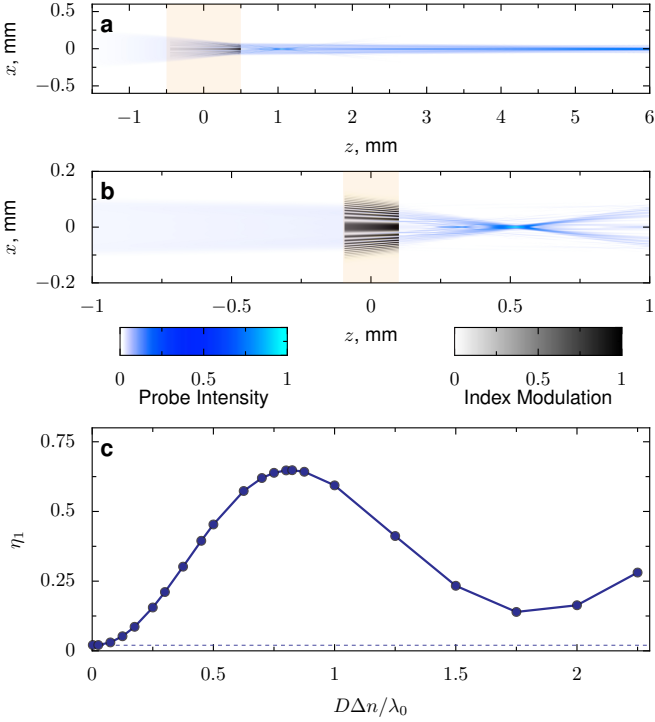


FIG. 3. Calculations (3D PPS) for a thick plasma lens, showing collimation (a) and focusing (b) depending on the initial probe focus position. (a) Probe (blue) near-collimated to focus at  $z = 6$  mm by lens formed in  $D = 1$  mm initial gas (orange), with  $\Delta n = 1.3 \times 10^{-4}$ ,  $\lambda_p = \lambda_0 = 400$  nm,  $f_A = 1$  mm, and  $f_B = 6$  mm; 81% of energy is within the focal spot at  $z = 6$  mm. (b) Focusing lens with  $D = 200$   $\mu\text{m}$  and  $\Delta n = 3.3 \times 10^{-3}$  for  $\lambda_0 = 800$  nm probe. Focal spot full-width-half-maximum is 2.2  $\mu\text{m}$ . Pumps have  $\lambda_p = 800$  nm,  $f_A = 0.5$  mm, and  $f_B = 3$  mm. (c) Efficiency ( $\eta_1$ ) for lens shown in (b), defined as probe energy a within 10- $\mu\text{m}$  radius at  $z = 0.5$  mm as  $\Delta n$  is varied between  $1 \times 10^{-5}$  and  $9 \times 10^{-3}$  for fixed  $D$ .

a collimated beam was produced from one with a tight focus. In Fig. 3b, a similar plasma lens focuses the incident beam, with more than 50% of the energy inside a 2  $\mu\text{m}$  spot. Figure 3c shows how the focusing efficiency of the optic in (b) decreases as the plasma density changes from its optimal value. Maximum efficiency occurs near where  $D/\lambda_0 = \Delta n$ , with smaller values of  $\Delta n$  producing minimal energy transfer to the  $m = 1$  order.

To capture the nonlinear dynamics of SVI, where high-intensity pulses propagate in an initially neutral gas, we use a numerical envelope equation solver [40, 41]. Our code [37] simulates the time evolution of the grating and pulses during the interaction, and includes the medium nonlinearity and group velocity dispersion, plasma recombination, and the effect of ionization induced by the pumps and probe on their own propagation. Figure 4 shows the plasma density (a) and focused probe profile (b) from a simulation where 0.65 mJ pumps form a plasma lens in nitrogen to focus a 1 ps, 60 mJ probe.

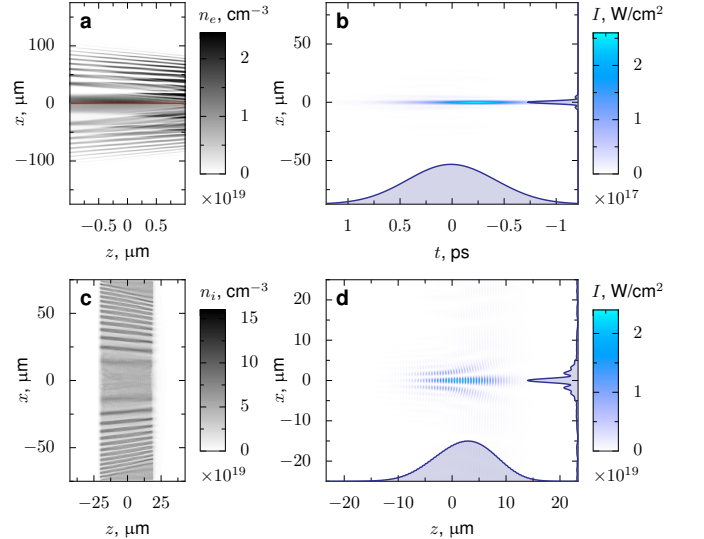


FIG. 4. Simulations of focusing by plasma lenses formed by SVI (a,b) and ponderomotive ion waves (c,d) using a nonlinear envelope equation solver (a,b) and 2D particle-in-cell simulations (c,d). (a) The density of plasma after passage of the pumps (upper half) and the probe (lower half) through a  $D = 200$   $\mu\text{m}$  column of molecular nitrogen. (b) The probe intensity at the  $z = 3$  mm focal spot. In (a,b), the pumps are 10 fs, 800 nm, 0.65 mJ pulses focused at  $z = 3$  mm and  $z = 0.5$  mm, and the probe is 1 ps, 800 nm, and 60 mJ. In (c,d), the pumps are 15 TW, 1  $\mu\text{m}$  pulses with 500 fs duration, the probe is a 100 TW, 1  $\mu\text{m}$  pulse with 40 fs duration, and the hydrogen plasma has  $D = 40$   $\mu\text{m}$  with an initial density density  $N = 0.045$  and electron temperature  $T_e = 100$  eV. (c) The ion density after both the pump and the probe have passed, and (d) the probe intensity near the focal spot.

Slight distortion and a reduction in intensity at the tail end of the probe indicate that this pulse is near the maximum tolerance of the plasma optic. With a diameter of just under 200  $\mu\text{m}$ , this lens operates at  $2.4 \times 10^{14}$  W/cm² and 230 J/cm², well above the limits of a glass optic.

A holographic plasma lens can also be created via the ponderomotive force in a fully ionized plasma, as shown by results from two-dimensional particle-in-cell simulations (EPOCH [42]) in Fig. 4cd. Here, the probe (100 TW) has much higher power and intensity than the pumps that formed the lens (15 TW) in a 40  $\mu\text{m}$  hydrogen plasma. The probe intensity within the grating reaches more than  $2 \times 10^{17}$  W/cm² without substantial distortion. Although the local electron density provides the index modulation, the plasma lens has an underlying ion density structure which changes shape slowly, helping maintain the overall structure even at high probe intensity. The 2D simulations underestimate the focal spot intensity that would be seen in a 3D system.

Plasma optics are useful only if they support higher intensity or energy flux in the probe than is required in the pumps that create them. For SVI, enhancement of

diffractive grating performance has been observed for intense probes [29], possibly because collisional ionization has a higher cross section than field ionization under the experimental conditions, enhancing already-ionized regions of the grating. As shown by these simulations, higher energy flux is also achievable, because the nonlinearity is primarily driven by intensity; if the probe stays below the ionization threshold, it will have little effect on the lens, and in principle a pulse 10 ps or longer can be efficiently diffracted. Although we have discussed collinear pumps, the beams do not have to lie along the same axis to create a hologram. The lens shape will be distorted, but it is possible to have both pumps and the probe at entirely separate angles while maintaining the viability of the lens as a focusing element.

In conclusion, we have shown that plasma nonlinearities can be used to create an efficient high-damage-threshold diffractive plasma lens. Simulations suggest that the intensity damage threshold of these lenses ranges from more than  $10^{14}$  W/cm<sup>2</sup> for the ionization mechanism to more than  $10^{17}$  W/cm<sup>2</sup> for the ponderomotive mechanism. The generality of holography means that holographic plasma optics can almost arbitrarily manipulate intense beams; these mechanisms are not limited to the creation of simple lenses.

This work was performed under the auspices of the U.S. Department of Energy by Lawrence Livermore National Laboratory under Contract DE-AC52-07NA27344. Support was provided by the LLNL-LDRD Program under Projects No. 20-ERD-057 and 21-LW-013, by NSF-BSF Grant No. 1803874, by NSF Grant No. PHY 1806911, and by DOE Grant No. DE-SC0017907.

Thomas, D. A. Callahan, S. W. Haan, J. D. Salmonson, S. Dixit, D. E. Hinkel, M. J. Edwards, B. J. MacGowan, J. D. Lindl, S. H. Glenzer, and L. J. Suter, Tuning the implosion symmetry of ICF targets via controlled crossed-beam energy transfer, *Phys. Rev. Lett.* **102**, 025004 (2009).

- [9] S. H. Glenzer *et al.*, Symmetric Inertial Confinement Fusion Implosions at Ultra-High Laser Energies, *Science* **327**, 1228 (2010).
- [10] G. Lehmann and K. H. Spatschek, Transient plasma photonic crystals for high-power lasers, *Phys. Rev. Lett.* **116**, 225002 (2016).
- [11] R. Kirkwood, D. Turnbull, T. Chapman, S. Wilks, M. Rosen, R. London, L. Pickworth, W. Dunlop, J. Moody, D. Strozzi, *et al.*, Plasma-based beam combiner for very high fluence and energy, *Nat. Phys.* **14**, 80 (2018).
- [12] C. Thaury, F. Quéré, J.-P. Geindre, A. Levy, T. Ceccotti, P. Monot, M. Bougeard, F. Réau, P. d’Oliveira, P. Audibert, R. Marjoribanks, and Ph. Martin, Plasma mirrors for ultrahigh-intensity optics, *Nat. Phys.* **3**, 424 (2007).
- [13] J. M. Mikhailova, A. Buck, A. Borot, K. Schmid, C. Sears, G. D. Tsakiris, F. Krausz, and L. Veisz, Ultra-high-contrast few-cycle pulses for multipetawatt-class laser technology, *Opt. Lett.* **36**, 3145 (2011).
- [14] P. Michel, L. Divol, D. Turnbull, and J. Moody, Dynamic control of the polarization of intense laser beams via optical wave mixing in plasmas, *Phys. Rev. Lett.* **113**, 205001 (2014).
- [15] K. Qu, Q. Jia, and N. J. Fisch, Plasma q-plate for generation and manipulation of intense optical vortices, *Phys. Rev. E* **96**, 053207 (2017).
- [16] D. Turnbull, C. Goyon, G. Kemp, B. Pollock, D. Mariscal, L. Divol, J. Ross, S. Patankar, J. Moody, and P. Michel, Refractive index seen by a probe beam interacting with a laser-plasma system, *Phys. Rev. Lett.* **118**, 015001 (2017).
- [17] D. Turnbull, P. Michel, T. Chapman, E. Tubman, B. Pollock, C. Chen, C. Goyon, J. Ross, L. Divol, N. Woolsey, *et al.*, High power dynamic polarization control using plasma photonics, *Phys. Rev. Lett.* **116**, 205001 (2016).
- [18] R. Wilson, M. King, R. Gray, D. Carroll, R. Dance, C. Armstrong, S. Hawkes, R. Clarke, D. Robertson, D. Neely, *et al.*, Ellipsoidal plasma mirror focusing of high power laser pulses to ultra-high intensities, *Phys. Plasmas* **23**, 033106 (2016).
- [19] A. G. MacPhee, D. Alessi, H. Chen, G. Cochran, M. R. Hermann, D. H. Kalantar, A. J. Kemp, S. M. Kerr, A. J. Link, T. Ma, *et al.*, Enhanced laser-plasma interactions using non-imaging optical concentrator targets, *Optica* **7**, 129 (2020).
- [20] A. Sakdinawat and D. Attwood, Nanoscale x-ray imaging, *Nature Photon* **4**, 840 (2010).
- [21] F. Krausz and M. Ivanov, Attosecond physics, *Rev. Mod. Phys.* **81**, 163 (2009).
- [22] A. Couairon and A. Mysyrowicz, Femtosecond filamentation in transparent media, *Phys. Rep.* **441**, 47 (2007).
- [23] J. Crane, G. Tietbohl, P. Arnold, E. Bliss, C. Boley, G. Britten, G. Brunton, W. Clark, J. Dawson, S. Fuchs, *et al.*, Progress on converting a NIF quad to eight, petawatt beams for advanced radiography, in *J. Phys. Conf. Ser.*, Vol. 244 (IOP Publishing, 2010) p. 032003.
- [24] A. Leblanc, A. Denoeud, L. Chopineau, G. Mennerat, P. Martin, and F. Quéré, Plasma holograms for ultrahigh-

\* edwards78@llnl.gov

- [1] D. Gabor, A new microscopic principle, *Nature* **161** (1948).
- [2] J. Kirz, Phase zone plates for x rays and the extreme uv, *J. Opt. Soc. Am.* **64**, 301 (1974).
- [3] H. Milchberg, Indestructible plasma optics, *Phys. Today* **72**, 70 (2019).
- [4] V. M. Malkin, G. Shvets, and N. J. Fisch, Fast compression of laser beams to highly overcritical powers, *Phys. Rev. Lett.* **82**, 4448 (1999).
- [5] Y. Ping, W. Cheng, S. Suckewer, D. S. Clark, and N. J. Fisch, Amplification of ultrashort laser pulses by a resonant Raman scheme in a gas-jet plasma, *Phys. Rev. Lett.* **92**, 175007 (2004).
- [6] A. Andreev, C. Riconda, V. Tikhonchuk, and S. Weber, Short light pulse amplification and compression by stimulated Brillouin scattering in plasmas in the strong coupling regime, *Phys. Plasmas* **13**, 053110 (2006).
- [7] M. R. Edwards, Q. Jia, J. M. Mikhailova, and N. J. Fisch, Short-pulse amplification by strongly-coupled stimulated Brillouin scattering, *Phys. Plasmas* **23**, 083122 (2016).
- [8] P. Michel, L. Divol, E. A. Williams, S. Weber, C. A.

- intensity optics, *Nat. Phys.* **13**, 440 (2017).
- [25] G. Lehmann and K. Spatschek, Plasma volume holograms for focusing and mode conversion of ultraintense laser pulses, *Phys. Rev. E* **100**, 033205 (2019).
- [26] I. Y. Dodin and N. J. Fisch, Storing, retrieving, and processing optical information by raman backscattering in plasmas, *Phys. Rev. Lett.* **88**, 165001 (2002).
- [27] Z.-M. Sheng, J. Zhang, and D. Umstadter, Plasma density gratings induced by intersecting laser pulses in underdense plasmas, *Appl. Phys. B* **77**, 673 (2003).
- [28] S. Sunsov, D. Abdollahpour, D. Papazoglou, and S. Tzortzakis, Femtosecond laser induced plasma diffraction gratings in air as photonic devices for high intensity laser applications, *Appl. Phys. Lett.* **94**, 251104 (2009).
- [29] L. Shi, W. Li, Y. Wang, X. Lu, and H. Zeng, Generation of high-density electrons based on plasma grating induced Bragg diffraction in air, *Phys. Rev. Lett.* **107**, 095004 (2011).
- [30] M. Durand, A. Jarnac, Y. Liu, B. Prade, A. Houard, V. Tikhonchuk, and A. Mysyrowicz, Dynamics of plasma gratings in atomic and molecular gases, *Phys. Rev. E* **86** (2012).
- [31] Y. Michine and H. Yoneda, Ultra high damage threshold optics for high power lasers, *Commun. Phys.* **3**, 1 (2020).
- [32] L. Friedland and A. Shagalov, Extreme driven ion acoustic waves, *Phys. Plasmas* **24**, 082106 (2017).
- [33] L. Friedland, G. Marcus, J. S. Wurtele, and P. Michel, Excitation and control of large amplitude standing ion acoustic waves, *Phys. Plasmas* **26**, 092109 (2019).
- [34] R. W. Wood, LIII. Phase-reversal zone-plates, and diffraction-telescopes, *Lond. Edinb. Dubl. Phil. Mag.* **45**, 511 (1898).
- [35] M. Sussman, Elementary diffraction theory of zone plates, *Am. J. Phys.* **28**, 394 (1960).
- [36] P. Yeh, *Introduction to Photorefractive Nonlinear Optics*, Wiley Series in Pure and Applied Optics (Wiley, 1993).
- [37] See Supplemental Material.
- [38] V. Levashov and A. Vinogradov, Analytical theory of zone plate efficiency, *Phys. Rev. E* **49**, 5797 (1994).
- [39] D. Woodbury, R. Schwartz, E. Rockafellow, J. K. Wahlstrand, and H. Milchberg, Absolute measurement of laser ionization yield in atmospheric pressure range gases over 14 decades, *Phys. Rev. Lett.* **124**, 013201 (2020).
- [40] T. Brabec and F. Krausz, Nonlinear optical pulse propagation in the single-cycle regime, *Phys. Rev. Lett.* **78**, 3282 (1997).
- [41] M. Mlejnek, E. M. Wright, and J. V. Moloney, Dynamic spatial replenishment of femtosecond pulses propagating in air, *Opt. Lett.* **23**, 382 (1998).
- [42] T. D. Arber, K. Bennett, C. S. Brady, A. Lawrence-Douglas, M. G. Ramsay, N. J. Sircombe, P. Gillies, R. G. Evans, H. Schmitz, A. R. Bell, and C. P. Ridgers, Contemporary particle-in-cell approach to laser-plasma modelling, *Plasma Phys. Contr. F.* **57**, 113001 (2015).

## Supplemental Material: Holographic Plasma Lenses

M. R. Edwards,<sup>1,\*</sup> V. R. Munirov,<sup>2</sup> A. Singh,<sup>2</sup> N. M. Fasano,<sup>3</sup> E. Kur,<sup>1</sup> N. Lemos,<sup>1</sup> J. M. Mikhailova,<sup>3</sup> J. S. Wurtele,<sup>2</sup> and P. Michel<sup>1</sup>

<sup>1</sup>*Lawrence Livermore National Laboratory, Livermore, California 94550*

<sup>2</sup>*University of California at Berkeley, Berkeley, California 94720*

<sup>3</sup>*Princeton University, Princeton, New Jersey 08544*

(Dated: May 14, 2021)

### SUPPLEMENTAL THEORY

The relative energy in the different orders of a thin zone plate can be calculated based on the distribution of index of refraction within each zone. As illustrated in Fig. 1c, the radii of boundaries between zones  $r_p$  are associated with  $\lambda/2$  phase shifts of light, from which follows

$$r_p^2 = p\lambda [f + p\lambda/4], \quad (1)$$

or  $r_p^2 \approx p\lambda f$  for  $p\lambda \ll f$ . In addition to the focal spot at  $f$ , a plane wave incident on a zone plate will be focused at points  $f_m = f/m$  for all integers  $m$ , including virtual (negative  $m$ ) foci; the relative energy in each focus depends on the exact distribution of index of refraction within the zones. If we assume that each pair of zones has the same variation of refractive index [ $n(\theta) = 1 - \delta(\theta) - i\kappa(\theta)$  where  $\theta = \pi r^2/(\lambda f)$  runs from 0 to  $2\pi$  for a zone pair], we can find the distribution of energy in each order [1] as  $P_m = |A_m|^2$  where

$$A_m = \frac{1}{2\pi} \int_0^{2\pi} e^{-\Gamma(\theta)+i[m\theta-\Phi(\theta)]} d\theta \quad (2)$$

and  $\Gamma(\theta) = 2\pi\kappa(\theta)d/\lambda$ ,  $\Phi(\theta) = 2\pi\delta(\theta)d/\lambda$ , and  $d$  is the thickness of the plate. Each pair of zones has the same area for  $p\lambda \ll f$ , so the above solution is independent of the number of zones. For an opaque binary plate [ $\Gamma(0 < \theta < \pi) = 0$ ,  $\Gamma(\pi < \theta < 2\pi) = \infty$  and  $\Phi = 0$ ], half of the incident energy is absorbed by the plate, and the remaining half is distributed among  $P_0$  (25%),  $P_{\pm 1}$  (10% each), and higher odd orders of  $P_m$  (5% total). If, as is the case for an ideal plasma zone plate, alternate zones are instead associated with a  $\pi$  phase shift, (a Rayleigh-Wood zone plate [2]), then  $P_{0,\pm 1,\pm 2,\pm 3,\dots} = [0, 41\%, 0, 4.4\%, \dots]$ , with no energy lost to absorption. The energy that can be transferred to order  $m = 1$  (convex) or  $m = -1$  (concave) is of primary concern for the creation of a lens. The ideal solution to Eq. 2 is a Fresnel lens [ $\Phi(\theta) = -\theta$ ], for which  $P_1 = 100\%$ , but since the response of the plasma-based index modulation to intensity is monotonic, it is not possible to turn the symmetric (across  $\theta$ ) index modulation into an asymmetric index modulation as would be required for a Fresnel lens.

### SIMULATION DETAILS

#### Paraxial Propagation Solver

The paraxial propagation solver (Figs. 2 and 3) solves the paraxial wave equation in the presence of an index modulation for a single-frequency infinite-duration beam:

$$(2ik_0\partial_z + \nabla_\perp^2)E(\mathbf{r}) = -2k_0^2E(\mathbf{r})\frac{\delta n(\mathbf{r})}{n_0}, \quad (3)$$

where the electric field ( $\tilde{E}$ ) is decomposed into envelope and high-frequency components as  $\tilde{E}(\mathbf{r}, t) = \frac{1}{2}E(\mathbf{r})\exp[i(k_0z - \omega_0t)] + \text{c.c.}$ ,  $k_0$  is the wavenumber,  $\omega_0$  is the frequency, and  $\mathbf{r}$  is the vector position. In our calculations, this equation is first evaluated for the pump beams, and an index modulation left by the pumps is calculated via  $\delta n = f(E)$ . For the results presented in this paper,  $f(E) \propto |E|^p$  with  $p = 4$  (Fig. 2, Fig. 3a) or  $p = 2$  (Fig. 3bc). The probe beam is then propagated according to Eq. 3 through the distribution of  $\delta n$  left by the pump beams. This approach does not resolve the time dynamics of plasma formation or the self-action via medium nonlinearity for the pumps or probe, but does allow efficient evaluation of the performance of arbitrary volumetric diffractive optics in the linear regime, which is where a plasma optic would be designed to operate. Parameters for simulations reported in this paper are presented in Table I.

TABLE I. Parameters for the Paraxial Propagation Solver

Parameter	Symbol	Fig. 2	Fig. 3a	Fig. 3b	Fig. 3c	Units
Pump wavelength	$\lambda_p$	400	400	800	800	nm
Pump focal position [A, B] <sup>a</sup>	$[f_A, f_b]$	$[-1, 1]$	$[6, 1]$	$[3, 0.5]$	$[3, 0.5]$	mm
Pump divergence [A, B]	$[\theta_A, \theta_B]$	$[3, 3]$	$[1, 6]$	$[2, 12]$	$[2, 12]$	°
Probe wavelength	$\lambda_0$	400	400	800	800	nm
Probe focal position	$f_0$	0.455	1	3	3	mm
Probe divergence	$\theta_0$	5	6	1.8	1.8	°
Maximum index modulation	$\Delta n$	$7.5 \times 10^{-3}$	$1.3 \times 10^{-4}$	$3.3 \times 10^{-3}$	$[10^{-5} - 0.009]$	-
Initial medium extent	$D$	40	1000	200	200	μm
Modulation formation exponent <sup>b</sup>	$p$	4	4	2	2	-
Transverse spatial resolution	$\Delta x, \Delta y$	143	120	160	160	nm
Transverse spatial extent	-	660	551	277	277	μm
Transverse grid points	$N_x, N_y$	4608	4608	1728	1728	-
Longitudinal spatial resolution, non-vacuum	$\Delta z$	2	50	5	5	μm
Longitudinal grid points, non-vacuum	$N_z$	20	20	40	40	-

<sup>a</sup> In  $z$ , where  $z = 0$  is at the center of the plasma. The plasma extends from  $z = -D/2$  to  $z = D/2$ .

<sup>b</sup> This is the parameter  $p$ , where  $\delta n = |E|^p$ .

### Nonlinear Envelope Equation Solver

The nonlinear envelope equation solver calculates the propagation of a light pulse under the paraxial and slowly varying envelope approximations. With the inclusion of nonlinear terms for plasma phase shift and absorption, ionization losses, and Kerr self-focusing, the governing equation is [7]:

$$\frac{\partial E}{\partial z} = \frac{i}{2k} \nabla_{\perp}^2 E - \frac{ik''}{2} \frac{\partial^2 E}{\partial t^2} - \frac{\sigma}{2} (1 + i\omega\tau) n_e E - W_{FI}(E) n_N \frac{U_i}{2|E|^2} + ik_0 n_2^T \left[ (1-f)|E|^2 + f \int_{-\infty}^{\infty} R(t-t')|E(t')|^2 dt' \right] \quad (4)$$

where the first term on the right hand side is the usual paraxial diffraction term and the second term represents group velocity dispersion ( $k'' = d^2 k / d\omega^2$ ). Note that the electric field here is assumed to be in the units of the square root of intensity. We use the following dispersion relation for nitrogen [8], where  $k_{[\mu\text{m}^{-1}]}$  is the wavenumber in radians/micron:

$$n(k) = 1 + \frac{5.1097029 \times 10^{-2}}{183.69459 - (k_{[\mu\text{m}^{-1}]} / 2\pi)^2} + \frac{2.12949 \times 10^{-6}}{7.74396 + (k_{[\mu\text{m}^{-1}]} / 2\pi)^2}. \quad (5)$$

The third term on the right hand side of Eq. 4 represents the phase shift and absorption by free electrons (density  $n_e$ ), where the inverse Bremsstrahlung cross section ( $\sigma$ ) is calculated locally with:

$$\sigma = \frac{ke^2\tau}{\omega m_e \varepsilon_0 (1 + \omega^2\tau^2)}. \quad (6)$$

The electron mass and charge are  $e$  and  $m_e$ , respectively, and  $\varepsilon_0$  is the vacuum permittivity. The collision time  $\tau$  is calculated based on local neutral density.

The fourth term represents loss of energy to the formation of the plasma, where  $W_{FI}$  is the field ionization rate and  $U_i$  is the ionization energy, and the fifth term contains both the instantaneous [ $n_2 = (1-f)n_2^T$ ] and time delayed contributions to the Kerr nonlinearity. Here,  $f$  is the relative contribution of the delayed component to the total  $n_2^T$ . The delayed response is approximated with a damped harmonic oscillator model [7]:

$$R(t) = H(t)\Omega^2 e^{-\Gamma t/2} \frac{\sin(t\sqrt{\Omega^2 - \Gamma^2/4})}{\sqrt{\Omega^2 - \Gamma^2/4}} \quad (7)$$

where  $H$  is the Heaviside step function and, following [7] for air, we have taken  $\Gamma = 26$  THz and  $\Omega = 20.6$  THz.

TABLE II. Parameters for the Nonlinear Envelope Equation Solver

Parameter	Symbol	Value	Units	Reference
Pump central wavelength	$\lambda_p$	800	nm	
Pump duration <sup>a</sup>	$\tau_p$	10	fs	
Pump focal position [A, B] <sup>b</sup>	$[f_A, f_b]$	[3, 0.5]	mm	
Pump divergence [A, B]	$[\theta_A, \theta_B]$	[2, 12]	°	
Pump energy [A, B]	-	[0.65, 0.65]	mJ	
Probe central wavelength	$\lambda_0$	800	nm	
Probe duration	$\tau_0$	1	ps	
Probe focal position	$f_0$	3	mm	
Probe divergence	$\theta_0$	1.5	°	
Probe energy	-	60	mJ	
Probe delay <sup>c</sup>	$\Delta\tau$	0.8	ps	
Neutral species	-	$N_2$	-	
Permitted ionized species	-	$N_2^+$	-	
Ionization energy	$U_i$	15.58	eV	
Initial neutral number density	$n_{N,0}$	$2.5 \times 10^{19}$	cm <sup>-3</sup>	
Initial neutral extent	$D$	200	μm	
Recombination parameter	$a$	$1.2 \times 10^{-13}$	m <sup>3</sup> /s	[3] <sup>d</sup>
Collision frequency <sup>e</sup>	$\tau_0$	$3.5 \times 10^{-13}$	s <sup>-1</sup>	[4, 5]
Instantaneous neutral nonlinearity	$n_2$	$7.4 \times 10^{-24}$	cm <sup>2</sup> /W	[6] <sup>f</sup>
Delayed response fraction	$f$	0.77	-	[6]
Transverse spatial resolution, vacuum <sup>g</sup>	$\Delta x, \Delta y$	340	nm	
Transverse spatial extent, vacuum	-	0.7	mm	
Transverse grid points, vacuum	$N_x, N_y$	2048	-	
Transverse spatial resolution, non-vacuum	$\Delta x, \Delta y$	340	nm	
Transverse spatial extent, non-vacuum	-	0.35	mm	
Transverse grid points, non-vacuum	$N_x, N_y$	1024	-	
Longitudinal spatial resolution, non-vacuum	$\Delta z$	1	μm	
Longitudinal grid points, non-vacuum	$N_z$	200	-	
Temporal resolution, pumps	$\Delta t$	0.31	fs	
Temporal extent, pumps	-	20	fs	
Temporal grid points, pumps	$N_t$	64	-	
Temporal resolution, probe	$\Delta t$	39	fs	
Temporal extent, probe	-	2.5	ps	
Temporal grid points, probe	$N_t$	64	-	

<sup>a</sup> Pulse durations are given in terms of the full-width-half-maximum (FWHM) of the Gaussian intensity envelope in time.

<sup>b</sup> In  $z$ , where  $z = 0$  is at the center of the plasma.

<sup>c</sup> Delay is the time separation between the peak of the pump pulses and the peak of the probe pulse.

<sup>d</sup> Also close to the value  $1 \times 10^{-13}$  m<sup>3</sup>/s from [4], where we have used values measured in air.

<sup>e</sup> For fully non-ionized conditions. The collision frequency is recalculated locally as neutral density changes.

<sup>f</sup> Due to the relatively short length of the propagation distance in the neutral medium, we do not observe a strong dependence on the exact value of this parameter for the performance of the optic.

<sup>g</sup> The simulation is divided into vacuum and non-vacuum components, where vacuum propagation can be spectrally solved for arbitrary propagation distance in a single step, and the non-vacuum propagation must be calculated with finite steps in  $z$  due to the medium response. The larger diameters of the beams outside the plasma requires a larger transverse size for the simulations.

The free electron density  $n_e$  evolves according to [9]:

$$\frac{\partial n_e}{\partial t} = W_{\text{FI}}(E)n_N + W_{\text{Ava}}(E)n_e - an_e^2. \quad (8)$$

where  $W_{\text{FI}}$  is the rate of field ionization,  $W_{\text{Ava}}$  is the rate of collisional (avalanche) ionization, and  $a$  is the recombination parameter. Since we consider here a single neutral species ( $N_2$ ) and a single ionized species ( $N_2^+$ ), the time derivative of the neutral density ( $n_N$ ) is simply:

$$\frac{\partial n_N}{\partial t} = -\frac{\partial n_e}{\partial t}, \quad (9)$$

and the initial neutral density is  $n_{N,0}$ . The rate of collisional ionization is:

$$W_{\text{Ava}} = \frac{\sigma}{U_i} |E|^2 \quad (10)$$

Note that we assume the electrons do not change position once formed, and the condition that the plasma remains frozen at the position of its formation sets a limit on the longest pulses and delay times that can be considered with this model.

For the parameters we consider here, the Keldysh parameter is in an intermediate regime, so to determine the field ionization rate we use the Perelomov, Popov, and Terentev (PPT) model with semi-empirical corrections based on experimental data [10–12]. The photoionization rate due to field ionization  $W_{\text{FI}}(I)$  in the PPT model is given, using atomic units, by [13]

$$W_{\text{FI}}(I) = \sqrt{\frac{6}{\pi}} |C_{n^*l^*}|^2 f_{lm} U_i \left[ \frac{2(2U_i)^{\frac{3}{2}}}{F} \right]^{2n^*-|m|-\frac{3}{2}} (1+\gamma^2)^{\frac{|m|}{2}+\frac{3}{4}} A_m(\omega, \gamma) \exp \left[ -\frac{2g(\gamma)(2U_i)^{\frac{3}{2}}}{3F} \right], \quad (11)$$

where  $n^* = Z/\sqrt{2U_i}$ ,  $l^* = n^* - 1$ ,  $Z$  is the ion charge,  $U_i$  is the ionization potential,  $F$  is the peak laser electric field (laser intensity  $I = 3.51 \times 10^{16} \text{ W/cm}^2$  for  $F = 1 \text{ au}$ ), and

$$|C_{n^*l^*}|^2 = \frac{2^{2n^*}}{n^* \Gamma(n^* + l^* + 1) \Gamma(n^* - l^*)}, \quad (12)$$

where  $\Gamma$  represents the gamma function,

$$f_{lm} = \frac{(2l+1)(l+|m|)!}{2^{|m|} |m|! (l-|m|)!}, \quad (13)$$

$$g(\gamma) = \frac{3}{2\gamma} \left[ \left( 1 + \frac{1}{2\gamma^2} \right) \sinh^{-1}(\gamma) - \frac{\sqrt{1+\gamma^2}}{2\gamma} \right], \quad (14)$$

$$A_m(\omega, \gamma) = \frac{4}{\sqrt{3\pi}} \frac{1}{|m|!} \frac{\gamma^2}{1+\gamma^2} \sum_{n>v}^{\infty} e^{-(n-v)\alpha(\gamma)} w_m \left( \sqrt{\frac{2\gamma(n-v)}{\sqrt{1+\gamma^2}}} \right), \quad (15)$$

$$w_m(x) = e^{-x^2} \int_0^x (x^2 - y^2)^{|m|} e^{y^2} dy, \quad (16)$$

$$\alpha(\gamma) = 2 \left[ \sinh^{-1}(\gamma) - \frac{\gamma}{\sqrt{1+\gamma^2}} \right], \quad (17)$$

$$v = \frac{E_i}{\omega} \left( 1 + \frac{1}{2\gamma^2} \right), \quad (18)$$

$$\gamma = \frac{\omega\sqrt{2U_i}}{F} = \frac{\omega Z}{Fn^*} = \frac{\omega F_0^{\frac{1}{3}}}{F} \quad (19)$$

where  $F_0 = (2U_i)^{\frac{3}{2}}$ .

For O<sub>2</sub> and N<sub>2</sub> we take  $l = m = 0$ . Thus, we have

$$W_{\text{FI}}(I) = \sqrt{\frac{6}{\pi}} |C_{n^*l^*}|^2 f_{00} U_i \left[ \frac{2(2U_i)^{\frac{3}{2}}}{F} \right]^{2n^*-\frac{3}{2}} (1+\gamma^2)^{\frac{3}{4}} A_0(\omega, \gamma) \exp \left[ -\frac{2g(\gamma)(2U_i)^{\frac{3}{2}}}{3F} \right], \quad (20)$$

$$f_{00} = 1, \quad (21)$$

$$A_0(\omega, \gamma) = \frac{4}{\sqrt{3\pi}} \frac{\gamma^2}{1 + \gamma^2} \sum_{n=[v]+1}^{\infty} e^{-(n-v)\alpha(\gamma)} w_0 \left( \sqrt{\frac{2\gamma(n-v)}{\sqrt{1+\gamma^2}}} \right), \quad (22)$$

$$w_0(x) = e^{-x^2} \int_0^x e^{y^2} dy = \frac{\sqrt{\pi}}{2} e^{-x^2} \operatorname{erfi}(x), \quad (23)$$

where  $\operatorname{erfi}$  is the imaginary error function. Following [12], for nitrogen N<sub>2</sub> and an 800 nm laser we take  $U_i = 15.58$  eV and  $Z_{\text{eff}} = 0.9$ .

We numerically evaluate Eq. 4 separately for the pumps and the probe using a standard method in reference frames that move with the group velocity of light [9]. Each pulse is specified in two transverse spatial dimensions and time; the distribution of light in transverse space and time is then updated by stepping through the propagation direction ( $z$ ). To account for the delayed probe, we have extended the standard treatment by solving Eq. 4 twice: once for the pump beams propagating in the initial neutral gas, and a second time for the probe. The probe solution takes as an initial condition the plasma distribution left after the pump, evolved according to Eq. 8 over the time delay between the pump and probe. The computational and physical parameters used for the simulations shown in Fig. 4ab are given in Table II.

Since the two parts of this calculation are connected only by the initial condition on the plasma distribution for the second part, we can use different time resolution for the pump and probe calculations. In vacuum regions, both the pumps and the probe can be propagated linearly over arbitrary distances, allowing a somewhat higher number of spatial grid points without prohibitive computational cost. Table II specifies the resolution and number of grid points used for time and all three dimensions of space, distinguishing where necessary between the pump and probe and between vacuum and non-vacuum propagation.

### Particle-in-Cell

Two-dimensional (2D) particle-in-cell (PIC) simulations were conducted with the code EPOCH [14] to study the formation of an ion-wave plasma lens (Figure 4cd) in a fully ionized initial plasma. The simulation box was 300  $\mu\text{m}$  long and 150  $\mu\text{m}$  wide ( $9000 \times 4500$  cells), containing the plasma lens and the probe focal spot. All lasers were introduced at the left boundary ( $z = -21 \mu\text{m}$ ) with gaussian temporal profiles and supergaussian (order 4) spatial profiles. The pumps and probe were all polarized in the  $x$  direction, i.e. their electric fields were within the 2D plane of the simulation. The simulation captured the creation of the lens by the pumps, the evolution of the plasma between the pumps and the probe, and the interaction of the probe beam with the plasma. The physical and computational parameters used for the PIC simulations are given in Table III.

\* edwards78@llnl.gov

- [1] J. Kirz, Phase zone plates for x rays and the extreme uv, *J. Opt. Soc. Am.* **64**, 301 (1974).
- [2] R. W. Wood, LIII. Phase-reversal zone-plates, and diffraction-telescopes, *Lond. Edinb. Dubl. Phil. Mag.* **45**, 511 (1898).
- [3] S. Tzortzakis, B. Prade, M. Franco, and A. Mysyrowicz, Time-evolution of the plasma channel at the trail of a self-guided IR femtosecond laser pulse in air, *Opt. Commun.* **181**, 123 (2000).
- [4] M. Feit and J. Fleck Jr, Effect of refraction on spot-size dependence of laser-induced breakdown, *Appl. Phys. Lett.* **24**, 169 (1974).
- [5] A. Couairon and A. Mysyrowicz, Femtosecond filamentation in transparent media, *Phys. Rep.* **441**, 47 (2007).
- [6] J. Wahlstrand, Y.-H. Cheng, and H. Milchberg, Absolute measurement of the transient optical nonlinearity in N<sub>2</sub>, O<sub>2</sub>, N<sub>2</sub>O, and Ar, *Phys. Rev. A* **85**, 043820 (2012).
- [7] M. Mlejnek, E. M. Wright, and J. V. Moloney, Dynamic spatial replenishment of femtosecond pulses propagating in air, *Opt. Lett.* **23**, 382 (1998).
- [8] E. R. Peck and B. N. Khanna, Dispersion of nitrogen, *J. Opt. Soc. Am.* **56**, 1059 (1966).
- [9] A. Couairon, E. Brambilla, T. Corti, D. Majus, O. de J. Ramírez-Góngora, and M. Kolesik, Practitioner's guide to laser pulse propagation models and simulation, *Eur. Phys. J. Spec. Top.* **199**, 5 (2011).
- [10] C. Guo, M. Li, J. P. Nibarger, and G. N. Gibson, Single and double ionization of diatomic molecules in strong laser fields, *Phys. Rev. A* **58**, R4271 (1998).

TABLE III. PIC Simulation Parameters

Parameter	Symbol	Value	Units
Pump wavelength	$\lambda_p$	1000	nm
Pump duration <sup>a</sup>	$\tau_p$	500	fs
Pump focal position [A, B] <sup>b</sup>	[ $f_A, f_B$ ]	[8, 0.2]	mm
Pump divergence [A, B]	[ $\theta_A, \theta_B$ ]	[0.7, 20]	°
Pump peak power [A, B]	-	[15, 15]	TW
Probe wavelength	$\lambda_0$	1000	nm
Probe duration	$\tau_0$	40	fs
Probe focal position	$f_0$	8	mm
Probe divergence	$\theta_0$	0.7	°
Probe peak power	-	100	TW
Probe delay <sup>c</sup>	$\Delta\tau$	1.1	ps
Plasma density	$n_e$	$5 \times 10^{19}$	cm <sup>-3</sup> <sup>d</sup>
Plasma extent	$D$	40	μm
Electron temperature	$T_e$	100	eV
Ion temperature	$T_i$	10	eV
Ion mass (atomic hydrogen)	$m_i$	1836	$m_e$ <sup>e</sup>
Spatial resolution	$\Delta x, \Delta z$	33.3	nm <sup>f</sup>
Temporal resolution	$\Delta t$	0.075	fs <sup>g</sup>
Particles per cell per species	-	10	-
Spatial extent, longitudinal	-	300	μm
Spatial extent, transverse	-	150	μm

<sup>a</sup> Pulse durations are given in terms of the full-width-half-maximum (FWHM) of the Gaussian intensity envelope in time.

<sup>b</sup> In  $z$ , where  $z = 0$  is at the center of the plasma.

<sup>c</sup> Delay is the time separation between the peak of the pump pulses and the peak of the probe pulse.

<sup>d</sup>  $N = n_e/n_c = 0.045$ .

<sup>e</sup> In units of the electron mass,  $m_e$ .

<sup>f</sup>  $\lambda_0/\Delta x = 30$ .

<sup>g</sup>  $\Delta t = 0.95\Delta x/(\sqrt{2}c)$ .

- [11] J. Wu, H. Zeng, and C. Guo, Comparison study of atomic and molecular single ionization in the multiphoton ionization regime, Phys. Rev. Lett. **96**, 243002 (2006).
- [12] A. Talebpour, J. Yang, and S. Chin, Semi-empirical model for the rate of tunnel ionization of N<sub>2</sub> and O<sub>2</sub> molecule in an intense Ti:sapphire laser pulse, Opt. Commun. **163**, 29 (1999).
- [13] Z. Song, Z. Zhang, and T. Nakajima, Transverse-mode dependence of femtosecond filamentation, Opt. Express **17**, 12217 (2009).
- [14] T. D. Arber, K. Bennett, C. S. Brady, A. Lawrence-Douglas, M. G. Ramsay, N. J. Sircombe, P. Gillies, R. G. Evans, H. Schmitz, A. R. Bell, and C. P. Ridgers, Contemporary particle-in-cell approach to laser-plasma modelling, Plasma Phys. Contr. F. **57**, 113001 (2015).